Journal of Korean Association of Crystal Growth
Vol. 9, No. 4 (1999) 387-395

Phase diagrams and stable structures of stranski-krastanov structure mode for III-V ternary quantum dots

Kazuo Nakajima, Toru Ujihara, Satoru Miyashita and Gen Sazaki
Institute for Materials Research, Tohoku University, Sendai 980-8577, Japan
(Received June 9, 1999)

Abstract The strain, surface and interfacial energies of III-V ternary systems were calculated for three kinds of structure modes: the Frank-van der Merwe (FM) mode, the Stranski-Krastanov (SK) mode and the Volmer-Weber (VW) mode. The free energy for each mode was estimated as functions of the thickness and composition or lattice misfit. Through comparison of the free energy of each mode, it was found that the thickness-composition phase diagrams of III-V ternary systems can be determined only by considering the balance of the free energy and three kinds of structure modes appear in the phase diagrams. The SK mode appears only when the lattice misfit is large and/or the lattice layer is thick. The most stable structure of the SK mode is a cluster with four lattice layers or minimum thickness on a wetting layer of increasing lattice layers. The VW mode appears when the lattice misfit is large and the lattice layer is thin and only in the InPSb/InP and GaPSb/GaP systems which have the largest lattice misfit of III-V ternary systems. The stable region of the SK mode in the GaPSb/GaP and InPSb/InP phase diagrams is largest of all because the composition dependence of the strain energy of these systems is stronger than that of the other systems. The critical number of lattice layers below which two-dimensional (2D) layers precede the three-dimensional (3D) nucleation in the SK mode at x = 1.0 depends on the lattice misfit.

1. Introduction

The growth of thin films has been categorized into three types, namely, the Frank-van der Merwe (FM) mode (layer-by-layer growth), the Stranski-Krastanov (SK) mode (the first layer or layers remain smooth and clusters form on top) and the Volmer-Weber (VW) mode (clusters form) [1]. These growth modes are deduced from equilibrium considerations of the energy balance between the surface energy and the interfacial energy for lattice-matched systems. For heteroepitaxial growth of highly strained structures, however, the elastic strain energy associated with epitaxial lattice misfit must be considered. Recently, these modes were deduced by taking into consideration the elastic energy, and equilibrium phase diagrams of the unspecific system were determined in function of the coverage and misfit [2, 3].

The SK mode has received much interest due to the emergence of new growth technology for fabricating self-assembling quantum dots [4-8]. In the SK mode of InGaAs quantum dots on a GaAs substrate, islandlike formation of InGaAs dots takes place with a very thin InGaAs wetting layer covering the substrate [4, 5]. In order to identify the kind of system in which quantum dots can easily be formed, we must determine the thickness-composition equilibrium phase diagrams of all the III-V ternary systems and understand how widely the region of the SK mode spreads. Daruka and Barabasi [3] determined the general coverage-lattice misfit phase diagrams for self-assembled quantum dots without using specific material constants. However, no phase diagrams have been reported for specific systems such as III-V compound semiconductors.

In this work, the free energy was calculated at every lattice layer for the three kinds of structures, i.e., a strained film on a substrate, a cluster on a strained film on a substrate and a cluster on a substrate, which represent the FM mode, the SK mode and the VW mode, respectively. The free energy for each structure was derived from the strain energy, the surface energy and the interfacial energy, and it was determined as functions of thickness and composition of the strained film and/or cluster. By comparison of the free energy of three structure modes, we determined thickness-composition phase diagrams of the SK mode for four III-V ternary systems, InPSb/InP, InAsSb/InAs, GaPSb/GaP, GaAsSb/GaAs. The (111) face was selected for this calculation. The area of the SK region was determined as a function of the lattice

misfit and the surface energy. The critical number of lattice layers below which two-dimensional (2D) layers precede the three-dimensional (3D) nucleation in the SK mode at x = 1.0 was determined as a function of the lattice misfit. The free energy of various types of the SK mode structure for the GaPSb on GaP system was calculated to determine the most stable structure of the SK mode.

2. Calculation method

The schematic geometry of a GaPSb strained film on a GaP substrate (the FM mode) and a GaPSb cluster on a GaP substrate (the VW mode) is given in Fig. 1. In this figure, the GaPSb/GaP system is used as an example of three kinds of structure mode. One lattice layer, whose thickness is equal to the lattice constant, is determined as a unit thickness of the film, and four lattice layers are designated as the unit thickness of the cluster. The total volume of the film is equal to that of the cluster. Figure 1 shows the fundamental structures for the case of one lattice layer.

The schematic geometry of a GaPSb strained film on a GaP substrate (the FM mode) and a GaPSb cluster on a GaPSb strained film on a GaP substrate (the SK mode) is given in Fig. 2. A cluster with four lattice layers on a film with one lattice layer is determined to be the fundamental structure of the SK mode. The total volume of the film with two lattice layers is equal to that of the cluster on the film with one lattice layer. Figure 2 shows the fundamental structures for the case of two lattice layers.

The excess free energy is derived from the difference between the final states as shown in Figs. 1 and 2 and the initial state. In this work, however, the total free energy of the initial state has the same value for all three structure modes because they are under the same initial conditions. Thus, only the total free energies derived from the final states of the three structure modes were considered and compared to determine the phase diagrams.

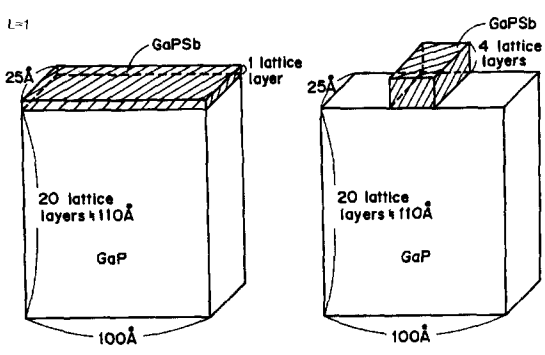

(a) Frank - van der Merwe mode (b) Volmer - Weber mode

Fig. 1. Schematic geometry of (a) GaPSb film on GaP substrate (the FM mode) and (b) a GaPSb cluster on GaP substrate (the VW mode) for the case of one lattice layer.

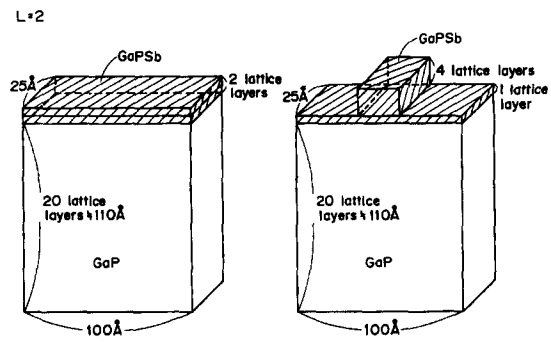

(a)Frank - van der Merwe mode (c) Stranski - Krastanov mode

Fig. 2. Schematic geometry of (a) GaPSb film on GaP substrate (the FM mode) and (b) a GaPSb cluster on GaPSb film on GaP substrate (the SK mode) for the case of two lattice layers.

The total free energy of each structure can be given as

$$G^t = G^{in} + G^{st} + G^{su} + G^{if}, \quad (1)$$

where G^t, G^{in}, G^{st}, G^{su} and G^{if} are the total free energy, the internal free energy, the strain energy, the surface energy and the interfacial energy, respectively. They are the energies of each structure in the final states, as shown in Figs. 1 and 2. The internal free energies for the three kinds of structures are almost equal if the total volume of each structure is equal. Hence, we can compare only the free energy, which is obtained by subtracting the internal free energy from the total free energy, in order to determine the phase diagram.

For this calculation, the sizes of the film, cluster and substrate are shown in Figs. 1 and 2. The substrate is 100 Å long, 25 Å wide and 20 lattice layers thick (≒110 Å). The strained film is coherently deformed on the substrate, and its thickness is n lattice layers. The shape of the cluster is rectangular and its size is 25 Å long, 25 Å wide and 4 lattice layers thick. The cluster is 1/4 the length of the substrate. For the SK mode, a cluster of this size is grown on n lattice layers for the fundamental structure of (n + 1) lattice layers.

In order to calculate the strain energy under the

assumption that each heterostructure has a coherent interface, we used the method which was developed by Nakajima *et al.* to calculate the precise stress distribution of an island layer on a substrate [9]. In this method, each composed layer is divided into many imaginary thin layers [9-16] and the face force and strain balance is considered over all the imaginary thin layers with coherent interfaces. Shear lag analysis [17, 18] was improved [9, 10] by considering imaginary thin layers and used to calculate the longitudinal stress distribution in the three kinds of structures. In order to estimate the internal force used in this calculation, the force and moment balance method [11-16, 19-21], which is useful for calculating the vertical stress distribution in the heterostructure, was used.

The elastic strain energy in the ith imaginary thin layer Ui can be calculated using

$$U_i = \frac{A_i d_i \sigma_i^2}{2E_i}, \tag{2}$$

where σ_i, E_i, A_i and di are the stress, Young's modulus, surface area and thickness of the ith imaginary thin layer. The total strain energy of each structure G^{st}, which includes the strain energies of the film, cluster and substrate, is given by

$$G^{st} = \sum_{i=1}^{m} U_i = \sum_{i=1}^{m} \frac{A_i d_i \sigma_i^2}{2E_i}, \tag{3}$$

where m is the total number of imaginary thin layers which constitute each structure.

On the surface between the vapor and solid phases, the surface energy per unit area gs can be given approximately by

$$\gamma_s = (1 - w/u)\, \Delta H_{v0} N_0^{2/3}, \tag{4}$$

where u is the number of nearest neighbors of an atom in the bulk of the solid and w is the number of neighbors in the solid of an atom on the face in question, ΔH_{v0} is the enthalpy of evaporation of the material at 0 K, and N_0 is the number of atoms per unit volume [22]. The argument used is that the surface energy is the energy needed to break all of the nearest-neighbor bonds across a given plane. The number of atoms per unit area N_s can be related to N_0 as follows:

$$N_s = N_0^{2/3}. \tag{5}$$

For III-V zincblende-type compounds, N_s can be given by

$$N_s = \frac{4}{\sqrt{3}a^2} \tag{6}$$

for the (111) face, where a is the lattice constant of the III-V compound [23].

For growth from vapor, ΔH_{v0} is given by the enthalpy of evaporation ΔH [24, 25] per mole as

$$\Delta H_{v0} = \frac{\Delta H}{2N_A}, \tag{7}$$

where N_A is Avogadro's number ($N_A = 6.023 \times 10^{23}$). Therefore, from eqs. (4)-(7), the surface energy G^{su} can be written as

$$G^{su} = A_s \gamma_s = \frac{A_s \Delta H}{2\sqrt{3}a^2 N_A} \tag{8}$$

for the (111) face, where As is the surface area of each structure.

In order to roughly calculate the interfacial energy G^{if} between the film and the substrate (the FM and SK modes) or that between the cluster and the substrate (the VW mode), the bonding ratio at the interface was calculated. When the lattice constant of the film and cluster a is larger than that of the substrate a_{sub} ($a \geq a_{sub}$), a is given by

$$a = k a_{sub}, \tag{9}$$

$$k = \Delta a/a + 1 = (a - a_{sub})/a_{sub} + 1 \qquad (k \geq 1), \tag{10}$$

where $\Delta a/a$ means the lattice misfit between the film (or cluster) and the substrate.

In this calculation, we assumed that at the interface all dangling bonds on the film or cluster side combine with dangling bonds on the substrate side. At the interface, the bonding ratio β_1 on the film or cluster side is given by

$$\beta_1 = 1, \tag{11}$$

and the bonding ratio β_2 on the substrate side can be expressed by

$$\beta_1 = \frac{1}{k}, \tag{12}$$

which means that 1/k dangling bonds combine. The interface energy per unit area γ_i can be given by

$$\gamma_i = (1 - \beta_1)\gamma_s + (1 - \beta_2)\gamma_{sub} = \left(1 - \frac{1}{\Delta a/a + 1}\right)\gamma_{sub}, \tag{13}$$

where γ_{sub} is the surface energy per unit area of the substrate. Therefore, from eqs. (8)-(13), the interfacial energy G^{if} can be written as

$$G^{if} = A_i\gamma_i = A_1\left(1 - \frac{1}{\Delta a/a + 1}\right)\frac{\Delta H_{sub}}{2\sqrt{3}a^2_{sub}N_A} \quad (14)$$

for the (111) face, where A_i is the interfacial area of each structure, and ΔH_{sub} is the enthalpy of evaporation per mole of the substrate. The interfacial energy given by eq. (14) is based on the condition that only the number of unsaturated dangling bonds or misfit dislocations at the heterointerface is taken into account.

In this work, a cluster is considered to be hemispherical in order to estimate more actually the surface energy of the SK and VW modes and the interfacial energy of the VW mode. The volume of the cluster is set up to be equal regardless of the shape of the cluster.

By using eq. (1), the free energy G^f can be derived by subtracting the internal free energy G^{in} from the total free energy G^t:

$$G^f = G^t - G^{in} = G^{st} + G^{su} + G^{if}. \quad (15)$$

From eqs. (3), (8), (14) and (15), we can calculate G^f of each structure, which are then compared with each the other to determine the SK phase diagrams.

3. Calculated results

3.1. Parameters used in the calculation

Table 1 contains the parameters used for the calculation of the strain energy. The shear modulus G is estimated using Young's modulus E and the Poisson ratio ν as follows:

$$G = E/2\ (1 + \nu). \quad (16)$$

The parameters of the ternary compounds are estimated from those of the binary compounds on the

Table 1
Input data for the strain energy calculation

	Young's modulus (GPs)	Poisson's ration	Shear modulus (GPa)	Lattice contant (Å)	Thermal expansion coefficient (10^{-6}/K)
Gap	102.8	0.31	39.2	5.4512	5.91
Reference	[26]	[26]		[28]	[26]
GaSb	63.2	0.31	24.1	6.0954	6.36
Reference	[26]	[26]		[29]	[26]
GaAs	85.3	0.312	32.6	5.6534	6.86
Reference	[27]	[27]		[29]	[30]
InP	60.7	0.36	22.3	5.8688	4.56
Reference	[26]	[26]		[26]	[26]
InSb	43.9	0.34	16.4	6.4794	5.11
Reference	[26]	[26]		[26]	[26]
InAs	51.4	0.36	18.5	6.0584	4.60
Reference	[26]	[13]		[29]	[31]

Table 2
Input data for the surface and interfacial energy calculation

Input data						Units
$T^F_{GaP} = 1740$	[26]	$T^F_{GaSb} = 985$	[26]	$T^F_{GaAs} = 1511$	[32]	T^F_{ij} (K)
$T^F_{InP} = 1333$	[26]	$T^F_{InSb} = 797$	[26]	$T^F_{InAs} = 1215$	[33]	
$\Delta S^F_{GaP} = 16.8$	[26]	$\Delta S^F_{GaSb} = 15.8$	[26]	$\Delta S^F_{GaAs} = 16.64$	[34]	ΔS^F_{ij} (cal/mol K)
$\Delta S^F_{InP} = 14.0$	[26]	$\Delta S^F_{InSb} = 14.32$	[26]	$\Delta S^F_{InAs} = 14.52$	[34]	
$\Omega^l_{GaP} = 2800 - 4.8T$	[26]	$\Omega^l_{GaSb} = 4700 - 6.0T$	[26]	$\Omega^l_{GaAs} = 5160 - 9.16T$	[36]	Ω^l_{ij} (cal/mol)
$\Omega^l_{InP} = 4500 - 4.0T$	[26]	$\Omega^l_{InSb} = 3400 - 12.0T$	[26]	$\Omega^l_{InAs} = 3860 - 10.0T$	[37]	
$\Omega^l_{PSb} = 25000 - 18.0T$	[35]	$\Omega^l_{AsSb} = 750$	[26]	$\Omega^l_{PAs} = 1500$	[26]	
$\Omega^l_{GaIn} = 2300$	[38]					
$\Omega^S_{GaP-GaSb} = 8000$	[26]	$\Omega^s_{GaP-GaAs} = 400$	[26]	$\Omega^s_{GaAs-GaSb} = 4500$	[26]	Ω^s_{ij-ik} (cal/mol)
$\Omega^s_{InP-InSb} = 5000$	[26]	$\Omega^s_{InP-InAs} = 400$	[26]	$\Omega^s_{InAs-InSb} = 2250$	[26]	
$\Omega^s_{GaP-InP} = 3500$	[26]	$\Omega^s_{GaSb-InSb} = 1900$	[26]	$\Omega^s_{GaAs-InAs} = 3300$	[38]	
$H^l_{Ga} = -64608$	[39]	$H^l_{In} = -55508$	[39]	$H^l_{Sb} = -79774$	[39]	H^l_i (cal/mol)
$H^l_P = -49584$	[39]	$H^l_{As} = -73166$	[40]			

assumption of its linearity for composition. The parameters used in the calculation of the surface and interface energy are listed in Table 2, where T is the absolute temperature.

3.2. Strain, surface and interfacial energy calculations for the InPSb/InP structure

The strain, surface and interfacial energies were calculated using eqs. (3), (8) and (14) for the (111) face of three kinds of InPSb/InP structures, the FM, SK and VW modes. The InPSb/InP system is selected as an example of III-V ternary systems studied in this work. Figure 3 shows the free energy such as the strain, surface and interfacial energies as a function of the composition of InSb, x in InP_{1-x} Sb_x at 27°C. The structures consist of three lattice layers.

The strain energy of the FM mode is the largest and that of the VW mode is the smallest. The strain energy increases with the composition of InSb; x increases or the lattice misfit increases. The surface energy of the FM mode is the smallest and that of the VW mode is the largest. The surface energy decreases slightly as the composition of InSb increases. The interfacial energy of the FM mode is equal to that of the SK mode, and that of the VW mode is the smallest. The interfacial energy increases as the composition of InSb increases. The surface energy is generally larger than the strain and interfacial energy, but the strain energy of the FM mode becomes larger than the surface energy as the lattice misfit increases. The interfacial energy is the smallest of all the energies even though the maximum value is used in this work. As shown in Fig. 3, the relationship between the surface energy and the strain energy is very important in determining the stable structure mode.

These energies were calculated for each structure with various lattice layers, and the free energy for each structure was derived from these energies. Figure 4 shows the free energy for the (111) face as a function of the composition of InSb, x in InP_{1-x} Sb_x, and it corresponds to the structure with 2.5 lattice layers. As shown in Fig. 4, the free energy of the FM mode is the smallest in the range of composition smaller than 0.6, and that of the VW mode is the smallest in the range of composition larger than 0.95. That is, the FM mode is the most stable between x = 0 and 0.6, and the VW mode is the most stable between x = 0.95 and 1.0 when the number of lattice layers is 2.5.

3.3. Thickness-composition phase diagrams for SK structure modes of III-V ternary compounds

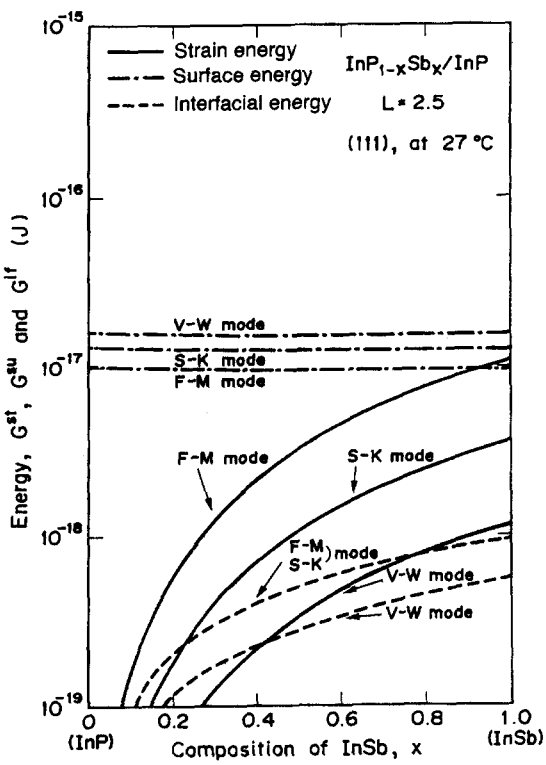

Fig. 3. Strain, surface and interfacial energies of InPSb/InP (111) structure with 2.5 lattice layers for the FM, SK and VW modes, as a function of InSb, x.

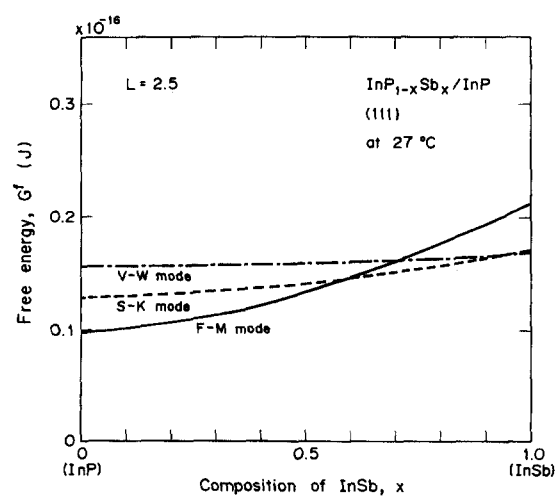

Fig. 4. Free energy of InPSb/InP (111) structure with 2.5 lattice layers for the FM, SK and VW modes, as a function of InSb, x.

By comparing the free energy of each mode at various thicknesses, we can determine the thickness-composition phase diagram for each structure mode. Figures 5-8 are the phase diagrams of the InPSb/InP, InAsSb/InAs, GaPSb/GaP, GaAsSb/GaAs systems, respectively. These phase diagrams are expressed as functions of the number of lattice layers L and the composition x. Figure 5 shows the phase diagram for $InP_{1-x}Sb_x$ layers grown on an InP substrate. When the lattice misfit or the composition of InSb is smaller, the FM mode appears most in the phase diagram. As the lattice misfit increases, the SK or VW mode becomes dominant. When the lattice misfit is large and the lattice layer is thin, the VW mode appears more easily than the SK mode does. The SK mode appears only for thick layers with large misfit.

Figure 6 shows the phase diagram for $InAs_{1-x}Sb_x$ layers grown on InAs substrates. The FM mode appears in most regions of the phase diagram. The SK mode appears as the lattice misfit increases and the layer becomes thicker. For the growth of InSb on InAs, the SK mode appears when the InSb lattice layer is thicker than 2.9 or about 19 Å. The VW mode does not appear in the InAsSb/InAs system. Figure 7

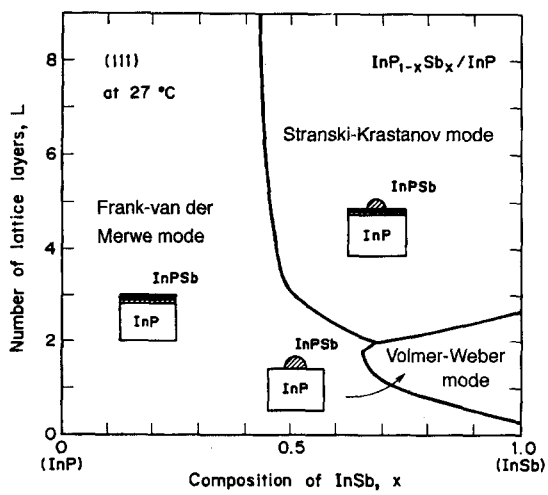

Fig. 5. Thickness-composition phase diagram of the FM, SK and VW modes for the InPSb/InP (111) structure.

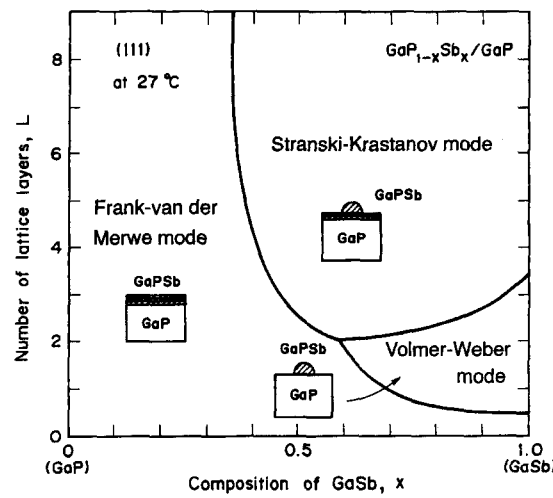

Fig. 7. Thickness-composition phase diagram of the FM, SK and VW modes for the GaPSb/GaP (111) structure.

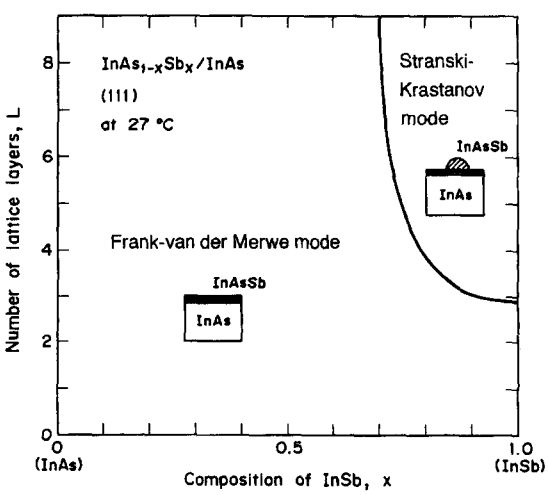

Fig. 6. Thickness-composition phase diagram of the FM and SK modes for the InAsSb/InAs (111) structure.

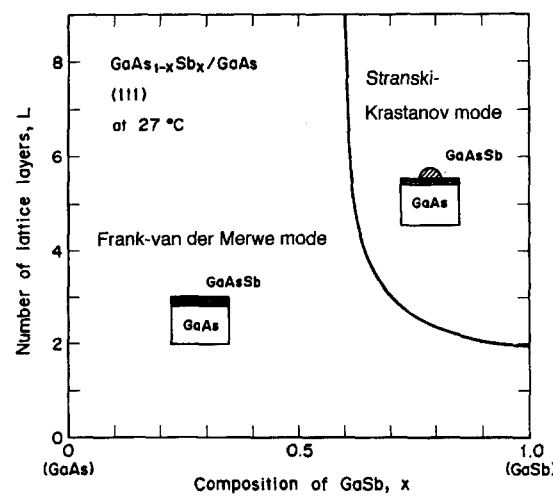

Fig. 8. Thickness-composition phase diagram of the FM and SK modes for the GaAsSb/GaAs (111) structure.

shows the phase diagram for $GaP_{1-x}Sb_x$ layers grown on GaP substrate. The SK mode appears in wide regions of the phase diagram. The VW mode appears in the region where the lattice misfit is large and the lattice layer is thin. The VW region of the GaPSb/GaP system is wider than that of the InPSb/InP system. Figures 8 shows the phase diagram for $GaAs_{1-x}Sb_x$ layers on GaSb substrate, in which the FM and SM modes appear and the VW mode does not appear.

3.4. *Effect of lattice misfit*

The lattice misfit is very important parameter for generating regions of the SK mode. Figure 9 shows the area of the SK region estimated from phase diagram 5 as a function of the lattice misfit. For the GaPAs/GaP and InPAs/InP systems, the SK mode does not appear in regions where the number of lattice layers is smaller than 9. The area of the SK region clearly depends on the lattice misfit, and it increases as the lattice misfit increases. The system in which the SK mode appears most easily is GaPSb/GaP.

Figure 10 shows the critical number of lattice layers below which two-dimensional (2D) layers precede the three-dimensional (3D) nucleation in the SK mode at x = 1.0, as a function of the lattice misfit. The critical number of lattice layers clearly depends on the lattice misfit. The InPSb/InP system has the smallest critical number of all.

3.5. *Stable structure of the SK mode*

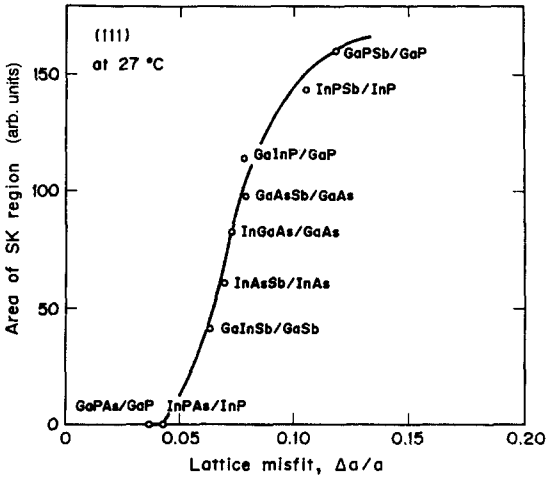

Fig. 9. Area of the SK region in the phase diagram of III-V ternary systems as a function of the lattice misfit.

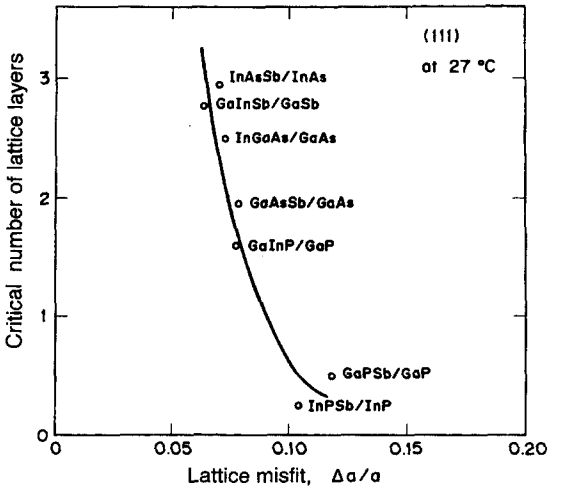

Fig. 10. Critical number of lattice layers below which two-dimensional (2D) layers precede the three-dimensional (3D) nucleation in the SK mode at x = 1.0 in the phase diagram of III-V ternary systems as a function of the lattice misfit.

As the number of lattice layers or thickness increases, however, many types of structure of the SK mode have possibility to appear as shown in Fig. 11. Figure 11 shows the growth path of the SK structure mode as the number of lattice layers increases. In order to understand the actual growth mechanism of the SK mode and the quantum dots, we must know which is the most stable structure and growth path.

The free energy was calculated for various types of the SK mode structure. The strain energy of the SKj

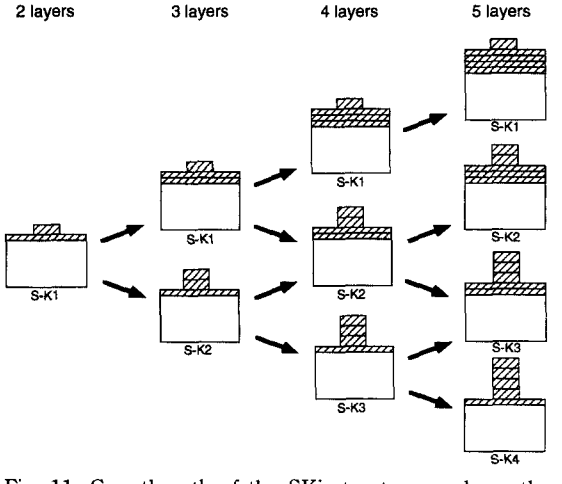

Fig. 11. Growth path of the SKj structure mode as the number of lattice layers increases. *j* corresponds to the cluster height.

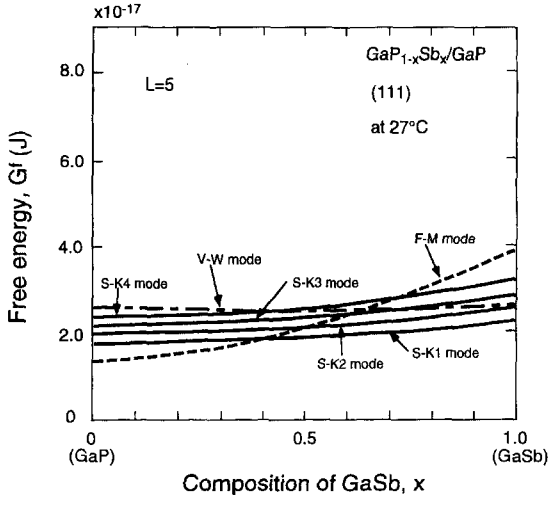

Fig. 12. Free energy of GaPSb/GaP (111) structure with five lattice layers for the FM, SKj and VW modes, as a function of GaSb fraction, x.

mode was calculated on the basis of the assumption that the wetting layer was compositionally graded. Figure 12 shows the free energy for the GaPSb on GaP system as a function of the composition of GaSb. The thickness is five lattice layers. The free energy of the SKj mode increases as the cluster height j increases all over the composition. As shown in Fig. 12, the FM mode is the most stable between x = 0.4 and 1.0 when the number of lattice layers is five. Then, the most stable structure of the SK mode is a cluster with four lattice layers or minimum thickness on a wetting layer with increasing lattice layers. The VW mode becomes more stable than the SKj mode as the cluster height j increases.

4. Discussion

This calculation of equilibrium phase diagrams is performed under equilibrium or static conditions and is not performed under growth conditions. The free energies of the FM mode, SK mode and VW mode are compared to determine the equilibrium phase diagrams. Exactly speaking, these phase diagrams indicate the stable regions of each structure mode by considering the balance of free energy. However, the regions of the structure mode almost correspond to the stable regions of the growth mode, except for the FM region right below the SK region. This FM region corresponds to the region below which two-dimensional (2D) layers precede the three-dimensional (3D) nucleation in the SK mode. In this study of the equilibrium phase diagrams of structure modes, this region is defined as the region of the FM structure mode because the structure of a layer-by-layer growth appears in this region.

By direct observation of self-assembled InAs islands deposited by molecular-beam epitaxy on GaAs (100), Leonard *et al.* [41] determined a critical thickness for the surface elastic relaxation of 1.5 monolayers (ML). This corresponds to the transition thickness from the FM mode to the SK mode. In this work, the transition thickness is 2.5 lattice layers, as shown in Fig. 10, and this value is about three times larger than the reported value of 1.5 ML. The relative strength of the surface energy has an important effect upon the stable region of each growth mode in the thickness-composition phase diagram. This effect was also pointed out by Daruka and Barabasi [3]. The surface energy can be more accurately estimated by considering the reconstruction of the dangling bond, the surface orientation dependence and the thickness dependent surface and interfacial energies. The phase diagram can be more precisely determined using such surface and interfacial energies. However, the present calculation is sufficient to identify the systems in which the SK mode appears more easily.

5. Conclusions

The strain, surface and interfacial energies were calculated for the FM, SK and VW modes, and the free energy was derived for each growth mode. By comparison of the free energies, it is found that the thickness-composition phase diagrams of III-V ternary systems can be determined only by considering the balance of the free energy and the three kinds of structure mode appear in the phase diagrams. In particular, the energy balance between the surface and strain energies is very important for determining the region of the SK mode. The SK mode appears only when the lattice misfit is large and/or the lattice layer is thick. The VW mode appears only when the lattice misfit is large and the lattice layer is thin and only in the InPSb/InP and GaPSb/GaP systems which have the largest lattice misfit of III-V ternary systems. The stable region of the SK mode in the GaPSb/GaP and InPSb/InP phase diagrams is largest of all because the composition dependence of the strain energies of

these systems is stronger than that of the other systems. The critical number of lattice layers below which two-dimensional (2D) layers precede the three-dimensional (3D) nucleation in the SK mode at x = 1.0 clearly depends on the lattice misfit. The InPSb/InP system has the smallest critical number of all. By comparison of the free energies of the several types of the SK structure, it is found that the most stable structure of the SK mode is a cluster with four lattice layers or minimum thickness on a wetting layer with increasing lattice layers.

Acknowledgments

The author wishes to thank Professors S. Ochiai and T. Kitamura of Kyoto University, and Associate Prof. S. Durbin of Tohoku University for helpful discussions.

References

[1] W. Seifert, N. Carlsson, M. Miller, M.-E. Pistol, L. Samuelson and L.R. Wallenberg, Prog. Cryst. Growth & Charact. 33 (1996) 423.
[2] I. Daruka and A.-L. Barabasi, Phys. Rev. Lett. 79 (1997) 3708.
[3] I. Daruka and A.-L. Barabasi, Appl. Phys. Lett. 72 (1998) 2102.
[4] D. Leonard, M. Krishnammurthy, C.M. Reaves, S.P. DenBaans and P.M. Petroff, Appl. Phys. Lett. 63 (1993) 3203.
[5] J.M. Moison, F. Houizay, F. Barthe, L. Leprince, E. Andre and O. Vatel, Appl. Phys. Lett. 64 (1994) 196.
[6] K. Mukai, N. Ohtsuka, M. Sugawara and S. Yamazaki, Jpn. J. Appl. Phys. 33 (1994) 1710.
[7] S.P. DenBaars, C.M. Reaves, V. Bressler-Hill, S. Varma, H. Weinberg and P.M. Petroff, J. Cryst. Growth 145 (1994) 721.
[8] J. Ahopelto, H. Lipsanen, M. Sopanen, Y.T. Kaljonen and H.E.M. Niemi, Appl. Phys. Lett. 65 (1994) 1662.
[9] K. Nakajima, K. Kitahara and S. Ochiai, Jpn. J. Appl. Phys. 35 (1996) 2605.
[10] K. Nakajima and S. Ochiai, Jpn. J. Appl. Phys. 34 (1995) 3000.
[11] K. Nakajima, J. Cryst. Growth 113 (1991) 477.
[12] K. Nakajima, J. Cryst. Growth 121 (1992) 278.
[13] K. Nakajima, J. Appl. Phys. 72 (1992) 5213.
[14] K. Nakajima, J. Cryst. Growth 126 (1993) 511.
[15] K. Nakajima, J. Cryst. Growth 137 (1994) 667.
[16] K. Nakajima and K. Furuya, Jpn. J. Appl. Phys. 33 (1994) 1420.
[17] J.M. Hedgepeth, NASA Technical Note D-882 (1961).
[18] S. Ochiai, K. Schulte and P.W.M. Peters, Composites Sci. & Technol. 41 (1991) 237.
[19] G.H. Olsen and M. Ettenberg, J. Appl. Phys. 48 (1977) 2543.
[20] Z. Feng and H. Liu, J. Appl. Phys. 54 (1983) 83.
[21] F. Cembali and M. Servidori, J. Appl. Cryst. 22 (1989) 345.
[22] J.C. Brice, Series of Monographs on Selected Topics in Solid State Physics, ed. E.P. Wohlfarth Vol. 12 (North-Holland, Amsterdam, 1973) p. 78.
[23] J.W. Cahn and R.E. Hanneman, Surf. Sci. 1 (1964) 387.
[24] K. Nakajima and K. Akita, J. Electrochem. Soc. 129 (1982) 2603.
[25] K. Nakajima and J. Okazaki, J. Electrochem. Soc. 132 (1985) 1424.
[26] H. Nagai, S. Adachi and T. Fukui, III-V Mixed Crystals, eds. R. Itoh, T. Kamiya and H. Kukimoto (Corona, Tokyo, 1988) p. 27.
[27] W.A. Brantley, J. Appl. Phys. 44 (1973) 534.
[28] H.C. Casey and F.A. Trumbore, Mater. Sci. Eng. 6 (1970) 69.
[29] G. Giesecke and H. Pfister, Acta Cryst. 11 (1958) 369.
[30] E.D. Pierron, D.L. Parker and J.B. McNeeley: J. Appl. Phys. 38 (1967) 4669.
[31] R. Bisaro, P. Merenda and T.P. Pearsall, Appl. Phys. Lett. 34 (1979) 100.
[32] C.D. Thurmond, J. Phys. Chem. Solids 26 (1965) 785.
[33] G.A. Antypas, J. Electrochem. Soc. 117 (1970) 1393.
[34] B.D. Lichter and P. Sommelet, Trans. AIME 245 (1969) 1021.
[35] K. Nakajima, K. Osamura and Y. Murakami, J. Jpn. Inst. Met. 37 (1973) 1276.
[36] J. A. Arthur, J. Phys. Chem. Solids 28 (1967) 2257.
[37] M.B. Panish and M. Ilegems, Progress in Solid State Chemistry, eds. H. Reiss and J.O. McCaldin Vol. 7 (Pergamon, Oxford, 1972) p. 39.
[38] K. Nakajima and S. Yamazaki, J. Cryst. Growth 74 (1986) 39.
[39] R.A. Shelton, Smithells Metals Reference Book, 7th edition, eds. E. A. Brandes and G. B. Brook (Butterworth-Heinemann, Oxford, 1992) p. 8-1.
[40] G.V. Samsonov, Handbook of the Physicochemical Properties of the Elements, ed. G. V. Samsonov (Oldbourne, London, 1968) p. 250.
[41] D. Leonard, K. Pond and P.M. Petroff, Phys. Rev. B 50 (1994) 11687.